



Continuous 2000 K droplet-to-particle synthesis

Xizheng Wang ^{1,†}, Zhennan Huang ^{2,†}, Yonggang Yao ¹, Haiyu Qiao ¹, Geng Zhong ¹, Yong Pei ³, Chaolun Zheng ³, Dylan Kline ^{4,5}, Qinqin Xia ¹, Zhiwei Lin ¹, Jiaqi Dai ¹, Michael R. Zachariah ⁵, Bao Yang ³, Reza Shahbazian-Yassar ^{2,*}, Liangbing Hu ^{1,*}

Aerosol spray coupled with high-temperature pyrolysis is an emerging technique for continuous manufacturing of nanomaterials at large scale that demonstrates extremely high production efficiency. Current aerosol spray techniques using a tube furnace can only attain a low temperature range (generally <1500 K), rendering limited products as well as inhomogeneous heating within the comparatively bulky furnace chamber (typical dimensions of ≥ 2 cm in diameter and ≥ 40 cm in length), which leads to difficulties in product quality control. Here we report a "droplet-to-particle" aerosol technique coupled with a high-temperature (~2000 K) micro-channel reactor, which provides \sim 100-times smaller dimensions compared to conventional tube furnaces, enabling homogeneous and high-temperature nanomaterial manufacturing. To demonstrate the unique capability of this carbonized wood micro-channel reactor, we successfully synthesized multielement high entropy alloy/oxide nanoparticles (which typically require a high temperature (2000 K) to achieve uniform elemental mixing) in a continuous and support-free manner. Droplets atomized from the multielement precursors fly through the micro-channels heated to 2000 K by Joule heating with a residence time of only tens of milliseconds with a high energy conversion efficiency (>95%), during which salt decomposition and particle nucleation/growth occur. The high temperature critically enables homogeneous mixing of elements in the resultant nanoparticles and the short residence time is key to suppress particle growth and agglomeration. Compared with the traditional aerosol spray pyrolysis, the carbonized wood reactor can achieve a record high temperature (>2000 K), a much shorter residence time (~tens of milliseconds), highly efficient, uniform heating, and provide a platform for continuous nanomaterial manufacturing for a broad range of applications.

Introduction

Nanoparticles have been explored for many important technological fields, such as energy storage, plasmonics, catalysis, and biomedical engineering, demonstrating unique and superior performance compared with their bulk counterparts [1–7]. The rapid

¹ Department of Materials Science and Engineering, University of Maryland, College Park, MD 20742, USA

² Department of Mechanical and Industrial Engineering, University of Illinois at Chicago (UIC), Chicago, IL 60607, USA

³ Department of Mechanical Engineering, University of Maryland, College Park, MD 20742, USA

⁴ Department of Chemical and Biomolecular Engineering, University of Maryland, College Park, MD 20742, USA

⁵ Department of Chemical and Environmental Engineering, University of California, Riverside, CA 92521, USA

st Corresponding authors.

E-mail addresses: Hu, L. (binghu@umd.edu), Shahbazian-Yassar, R. (rsyassar@uic.edu).

[†] These authors contributed equally to this work.

and scalable manufacturing of these nanomaterials is critical to enable wide applications but still remains a challenge. Aerosol spray pyrolysis is a powerful "droplet-to-particle" nanomanufacturing method that employs atomized solution-based precursors by pumping an aerosol flow through a heating zone continuously for large-scale production of nanoparticles in various states [8–12]. A variety of compounds, including metals [13], metal oxides [14,15], and carbon-based materials [16,17], have been synthesized using aerosol spray pyrolysis, which demonstrates several advantages including good scalability, low cost, high yield, simple operation, and the production of a wide diversity of materials with different stoichiometry, morphology, porosity, particle size, etc. [8,16,18]. However, current aerosol spray pyrolvsis techniques typically rely on a tube furnace as the heating element, which generally can reach temperatures of just <1500 K and tends to be overly bulky (diameter ≥ 2 cm, length ≥ 40 cm) for nanomaterial synthesis, resulting in low heating efficiency and poor quality control [19-24].

In this work, we introduce a "droplet-to-particle" aerosol spray synthesis method that overcomes these limitations by coupling the aerosol generator with a record-high temperature ($\sim\!2000~\rm K$) micro-channel reactor to achieve homogeneous and rapid nanomaterial manufacturing. By employing this continuous aerosol flow technique, substrate-free products can be collected for large-scale high-temperature nanomaterial manufacturing. The newly developed continuous 2000 K aerosol synthesis technique has the following advantages: (1) each micro-channel has a diameter of $\sim\!200~\mu m$ and a length of $\sim\!4~mm$, which is $\sim\!100$ -times smaller compared with the dimensions of a typical tube furnace chamber. (2) Such compact size

enables more homogenous heating and a significantly reduced residence time of only tens of milliseconds. (3) The microchannel reactor is triggered by electrical Joule heating, which can easily achieve a temperature of >2000 K in a highly efficient manner (>90% conversion from the input power to radiation). (4) The size of the as-synthesized nanoparticles can be tailored by the kinetic control of the process (e.g., temperature, precursor concentration). (5) Such a superior heating capability (high temperature, tens of milliseconds duration, and uniform heating in the micron-sized channels) enables the continuous synthesis of process-demanding nanomaterials, such as high entropy alloy (HEA) and high entropy oxide (HEO) nanoparticles. Note that HEAs/HEOs have recently emerged as chief contenders in a broad range of applications, including catalysis and energy storage [25-30], and their synthesis critically depends on achieving high temperatures and short residence times to enable homogeneous mixing of elements and suppressed particle growth/agglomeration, respectively. Therefore, we believe our carbonized wood micro-channel reactor may be ideal for the synthesis of such materials.

Results and discussion

In a typical synthesis (Fig. 1a), we used a collision nebulizer to generate an aerosol stream of droplets as small as 1 μ m in diameter (see Supporting Information for more details). Metal salt precursors in the aerosolized solution are homogeneously mixed in the resulting droplets, which are then propelled by the argon carrier gas through the micro-channel of the carbonized wood reactor. Upon the application of an electrical current to the reactor,

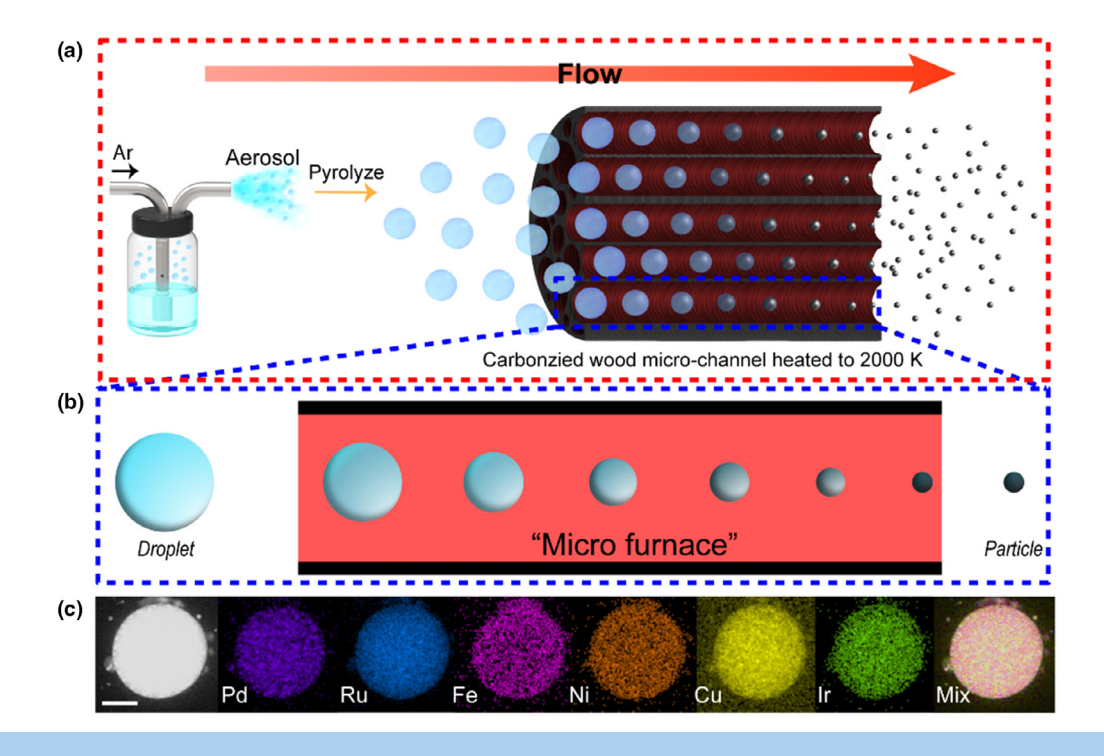


FIGURE 1

(a) Schematic of the droplets transporting through the carbonized wood micro-channels heated to 2000 K via the carrier gas. (b) Magnified schematic view of the droplet-to-particle evolution in an individual wood micro-channel, which serves as a micro furnace. (c) HAADF-STEM image and HAADF-EDS elemental maps of HEA PdRuFeNiCulr nanoparticles. Scale bar: 200 nm.

the droplet within its interior are effectively heated to 2000 K almost instantaneously due to their small size and the confined dimensions of the wood micro-channels. The high temperature drives the decomposition of the metal salt precursors and the formation of nanoparticles with a uniform solid-solution phase (Fig. 1b). With this technique, we were able to synthesize homogeneously mixed HEA PdRuFeNiCuIr nanoparticles in a continuous manner, as confirmed using the high-angle annular darkfield scanning transmission electron microscopy (HAADF-STEM) and energy dispersive X-ray spectroscopy (HAADF-EDS) mapping, which demonstrates the uniform mixing of all six elements (Fig. 1c).

Balsa wood, one of the lightest trees in the world with an approximately 73% void volume [31], was carbonized for use as the micro-channel reactor (Fig. S1). The individual vessel channels of the balsa wood can be seen by the naked eye (Fig. 2a) and provide ideal geometries for the aerosol droplets to pass through for particle synthesis. These numerous oval-shaped vessel channels that run along the tree growth direction (Fig. 2b, c) feature an average effective diameter of $\sim\!200\,\mu\text{m}$, which is $\sim\!200$ -times larger than the droplet sizes of the generated aerosol ($\sim\!1\,\mu\text{m}$), but 100-times smaller than a conventional tube furnace. Detailed scanning electron microscopy (SEM) images of the carbonized wood micro-channels at different magnifications

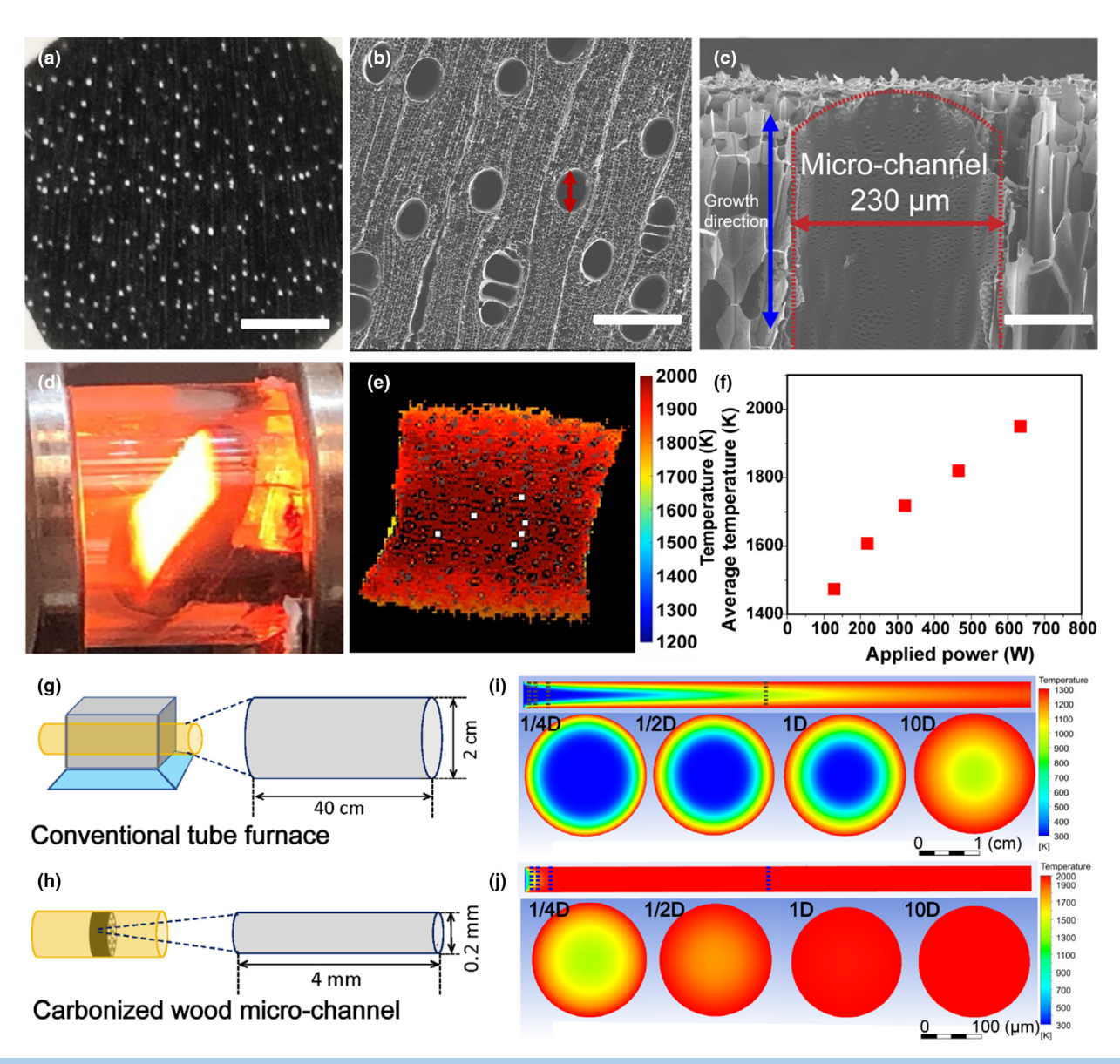


FIGURE 2

(a) Photograph of the carbonized balsa wood, in which the bright dots are from the passage of light through the open channels. Scale bar: 3 mm. (b) Topview SEM image of the wood micro-channels, looking down the length of the tree growth direction. Scale bar: 0.5 mm. (c) Cross-sectional view SEM image of a wood micro-channel. Scale bar: 100 μ m. (d) Photograph of the carbonized wood heated to 2000 K. (e) Temperature measurement of the carbonized wood heated to 2000 K. (f) Average temperature of the carbonized wood vs. the applied power. (g) Schematic of a conventional tube furnace. (h) Schematic of the carbonized wood micro-channel. (i) Temperature distribution of the 1300 K conventional tube furnace down its length and at cross-sections equal to $\frac{1}{4}$ -, $\frac{1}{2}$ -, and 10-times the diameter of the tube. (j) Temperature distribution of the carbonized wood micro-channel heated to 2000 K down its length and at cross-sections equal to $\frac{1}{4}$ -, $\frac{1}{2}$ -, and 10-times the diameter of the wood micro-channel.

are shown in Fig. S2. We can also cut the wood perpendicular to the tree growth direction at different lengths in order to tune the residence time of the aerosol droplets in the wood microchannels from several milliseconds to tens of milliseconds. During nanoparticle synthesis, a constant electrical power is applied to the carbonized wood to provide Joule heating (Fig. 2d) in a highly efficient manner (>90% conversion). The resulting temperature distribution in the wood is shown in Fig. 2e, easily reaching 2000 K, as measured by a pyrometer (see details in the Supporting Information) [32]. Furthermore, we can control the temperature by tuning the applied power (Figs. 2f and S3). When the applied power is over \sim 600 W, the temperature of the wood can be as high as \sim 2000 K.

Besides the higher temperature limit, the micro furnace of the wood micro-channels is far superior to conventional furnaces in terms of its ability to achieve a significantly decreased residence time. Under the same flow rate, the residence time of the aerosol droplets in a conventional furnace can be 2–3 orders of magnitude higher than that in the wood micro-channels. For example, the residence time of the aerosol at a flow rate of 5 L/min in a conventional furnace with a length of 40 cm is $\sim\!1.6$ seconds while that in a wood micro-channel with a length of $\sim\!4$ mm is only $\sim\!16$ milliseconds. In addition, it is likely that prolonged heating could lead to further growth of the nanoparticles [27]. With the higher temperature limit of the micro-channel reactor, the reaction rate will be greatly increased and thus the reaction can be completed in a shorter residence time. A shorter residence time can also prevent particle sintering due to less accumulated heat

Moreover, the heating efficiency of the carbonized wood is much higher than that of a conventional furnace due to the significantly reduced dimensions. Comparisons of the dimensions of a conventional tube furnace and the carbonized wood micro-channel are illustrated in Fig. 2g and 2h, respectively. The 100-times smaller dimensions of the wood micro-channel should result in more efficient and uniform heating. To determine whether this is the case, we conducted simulations on the temperature distributions along the tube furnace (based on the maximum temperature that the furnace could achieve (1300 K)) and carbonized wood micro-channel (based on 2000 K), respectively. Side views of the simulated objects are shown in Fig. 2i for the conventional furnace (detailed in Figs. S4) and 2j for the micro-channel reactor (detailed in Fig. S5) with the same carrier gas inlet velocity of 0.265 m/s. The temperature distribution simulations show that the temperature can increase to 2000 K in the carbonized wood microchannel in less than 1 ms (Fig. 2j), while for the conventional furnace the temperature increase is much more sluggish (Fig. 2i). Selected simulation results of the temperature profiles along the cross-section of the conventional furnace and the wood micro-channel at distances along their lengths equal to 1/4-, 1/2-, 1-, and 10-times the diameter of each object are also shown in Fig. 2i and Fig. 2j, respectively. In Fig. 2i, at the length of \sim 0.5 cm (corresponding to $\frac{1}{4}$ of the conventional furnace's diameter), the temperature at the center of the cross-section is only \sim 350 K. Even at a length of \sim 20 cm (10-times the diameter of the furnace), the temperature at the center of the cross-section is only \sim 900 K. However in Fig. 2j, at \sim 50 µm down the length of the micro-channel (equal to 1/4 of the diameter), the temperature at the center of the cross-section reaches \sim 1400 K. At the length of \sim 200 μm of the micro-channel (equivalent to its diameter), the temperature at the center of the cross-section reaches \sim 2000 K. In addition, when the temperature of the wood micro-channel is 2000 K, the carrier gas can be heated to \sim 2000 K within 0.1 milliseconds while the aerosol droplets can be heated to \sim 2000 K within 1 millisecond (Fig. S6a). In this case, the heating rate of argon can be as high as 10^7 K/s and the heating rate of the aerosol can be as large as 10^5 – 10^6 K/s. The hightemperature argon will accelerate the heating of the aerosol since there is a positive temperature gap between them. In contrast, for the conventional furnace, although it seems that the aerosol can be heated up to 1300 K within 0.01 s, the heating of the argon is much slower (Fig. S6b). The negative temperature gap between them leads to less efficient heating of the aerosol particles and thus the actual temperature increase of the aerosol is slowed.

Our micro-channel reactor demonstrates several distinct features compared to the conventional tube furnace, as outlined in Table 1: (1) tube size reduction by 100-times, which leads to (2) better temperature uniformity; (3) higher temperature limit driven by electrical Joule heating; (4) significantly increased reaction rate due to the high temperature; (5) 2–3 orders of reduced duration time to suppress nanoparticle segregation and sintering and (6) the strong capability to synthesize HEA/HEO particles.

In addition, besides balsa wood, other types of carbon-based materials with micron-sized channels can be used as microreactors for the continuous synthesis including: (1) different wood species with assorted channel geometries (e.g., poplar wood with channel diameter on the order of $\sim\!100~\mu m)$; (2) wood with artificially drilled pores to achieve the desired pore size and numbers; (3) highly crystalline 3D printed carbon frameworks, e.g., reduced graphene oxide (rGO).

A wide variety of materials can be synthesized via the carbonized wood reactor so long as the precursors can be atomized into droplets. As proof-of-concept, we synthesized and characterized HEA and HEO nanoparticles, which can primarily be obtained by rapid high-temperature heating and cooling [27]. Equal amounts of $\mathrm{MCl_xH_y}$ (M = Co, Ni, Pd, Ru, Ir) precursors (0.05 M in ethanol) were atomized into droplets. After passing through the carbonized wood micro-channel reactors heated to 2000 K via the carrier gas, spherical CoNiPdRuIr HEA nanoparticles were synthesized (Figs. 3a, S7). Since the HEA nanoparticles are derived from droplets that feature a log-normal distribution, the size of the particles also demonstrates a log-normal distribu-

TABLE 1

Comparison between a conventional tube furnace and our 2000 K microchannel reactor for aerosol spray pyrolysis.

Comparison	Conventional	Micro-channel reactor
Channel diameter	≥2 cm	\sim 200 μm
Channel length	≥40 cm	Highly tunable, \sim mm
Temperature distribution	Not uniform	Uniform
Temperature limitation	<1500 K	≥2000 K
Reaction rate	Low	High
Residence time	>1 s	\sim tens of milliseconds
Capability to synthesize HEA	Weak	Strong

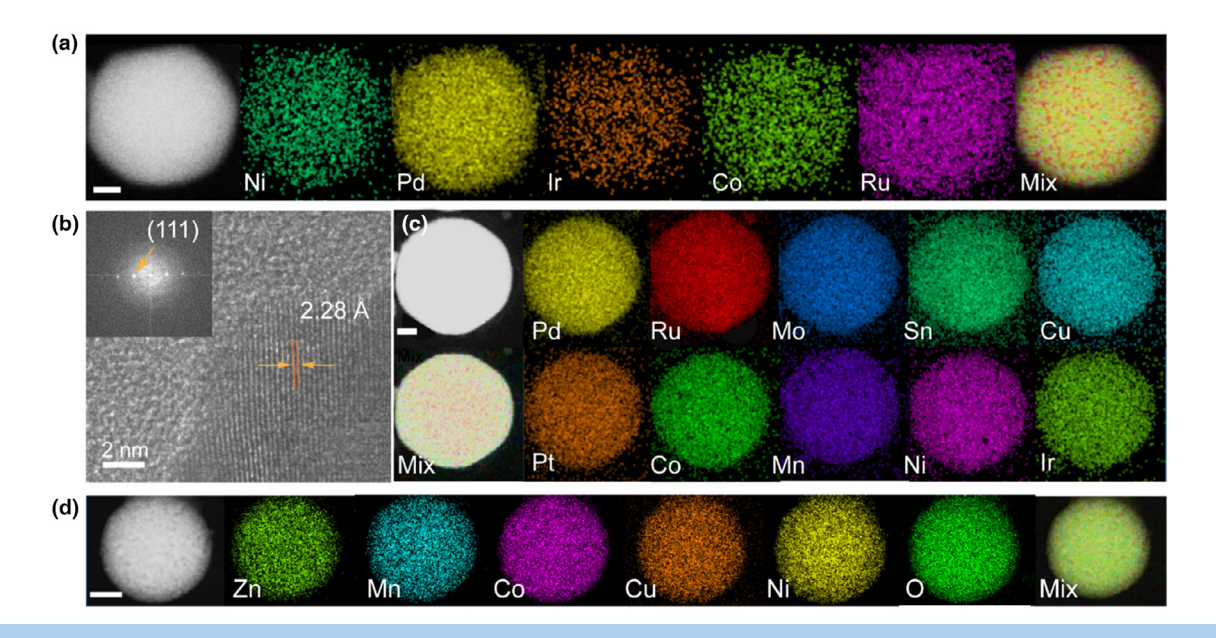


FIGURE 3

(a) HAADF-STEM image and HAADF-EDS elemental maps of a quinary HEA nanoparticle (CoNiPdRulr). Scale bar: 20 nm. (b) High-resolution TEM image with fast Fourier transform analysis (inset) of the CoNiPdRulr HEA-NPs, showing a typical FCC structure. (c) HAADF-STEM image and HAADF-EDS elemental maps of a ten-element HEA nanoparticle (AuCoCulrPtMnMoNiPdRu). Scale bar: 20 nm. (d) HAADF-STEM image and HAADF-EDS elemental maps of a quinary HEO nanoparticle (ZnCoMnNiCuO_x). Scale bar: 100 nm.

tion, with a mean diameter of \sim 160 ± 5 nm (Fig. S7). More than 75% of the particles have diameters less than 200 nm. Additionally, elemental analysis shows that the different elements are evenly dispersed within the particles (Fig. 3a). No apparent elemental segregation or phase separation was observed. To avoid the possibility of oxidation, argon is used as the carrier gas which flows through the synthesis system. After synthesis, the HEA nanoparticles are collected in the glovebox and stored properly in Ar to avoid oxidation. Using high-resolution transmission electron microscopy (TEM), we determined the lattice spacing of a CoNiPdRuIr nanoparticle was 2.28 Å, which matches well with the typical FCC metal structure of the (111) plane (Fig. 3b). As a comparison, we atomized the same precursors and passed them through a conventional furnace, which was set to 1300 K. However, using this method, the particles demonstrated severe phase separation between PdRuIr and CoNi (Fig. S8). This observation proves that the superior heating capability of the wood micro-channel reactor enables HEA formation.

Our droplet-to-particle synthesis also enables the formation of more complex HEA materials that have been challenging to synthesize by traditional methods. Previously reported HEA particles have been primarily composed of noble metals [27,33]. However, HEA composites composed of all transition metals have superior mechanical properties, but are commonly produced by welding from bulk metal alloys which is cost-prohibitive [34,35]. Using our technique of transporting an aerosol through the 2000 K carbonized wood micro-channel reactor, we demonstrate the ability to synthesize substrate-free, homogeneously mixed HEA nanoparticles composed of all transition metals (e.g., CrMnFe-CoNi; Fig. S9). This technique can also be extended to the preparation of even more complex HEA nanoparticles, such as those containing ten dissimilar elements (Au, Co, Cu, Ir, Pt, Mn, Mo, Ni, Pd, Ru). We note that there are significant physicochemical

property differences in these elements in terms of their atomic radii, melting/boiling points, and preferred crystal structure, as well as their metal precursors, which demonstrate different chemical reduction potentials and physical decomposition temperatures (Table S1). Despite these challenges, the combination of the aerosol spray with our micro-channel reactor enables the homogenous distribution of the ten elements within the resulting HEA nanoparticles (Fig. 3c).

Besides HEAs, we were also able to successfully synthesize HEO nanoparticles using metal nitrates as precursors. Similar to the preparation of HEAs, equal amounts of $M_x(NO_3)_y$ (M = Mn, Co, Ni, Cu, Zn) precursors (0.05 M in ethanol) were atomized into droplets. After rapidly transporting through the microchannel reactor, solid ZnMnCuCoNiO_x HEO particles formed with homogeneously distributed elements (Fig. 3d). The HEO particle size analysis featured a log-normal distribution with a mean diameter of $\sim 184 \pm 15$ nm (Fig. S10). X-ray diffraction (XRD) showed that the five elements (Mn, Co, Ni, Cu, Zn) were entropy-stabilized on the cation sublattice in a single-phase rock salt structure (Fig. S11) [36].

In all syntheses, we observed no aggregation between particles. It has been reported that the characteristic coagulation time is $\sim\!100\,\mathrm{s}$ when synthesizing 100 nm particles using a conventional atomizer that produces droplets in a concentration of $\sim\!10^6$ particles/cm³ [8]. The estimated characteristic coagulation time is 5–6 orders of magnitude longer than the residence time in the micro-channel reactor. Therefore no significant aggregation should be expected.

A detailed schematic of this droplet-to-particle synthesis made possible by the carbonized wood micro-channel reactor is illustrated in Fig. 4a. After the precursor solutions are atomized into droplets, they are transported via the carrier gas into the natural channels of the carbonized wood heated to 2000 K where they

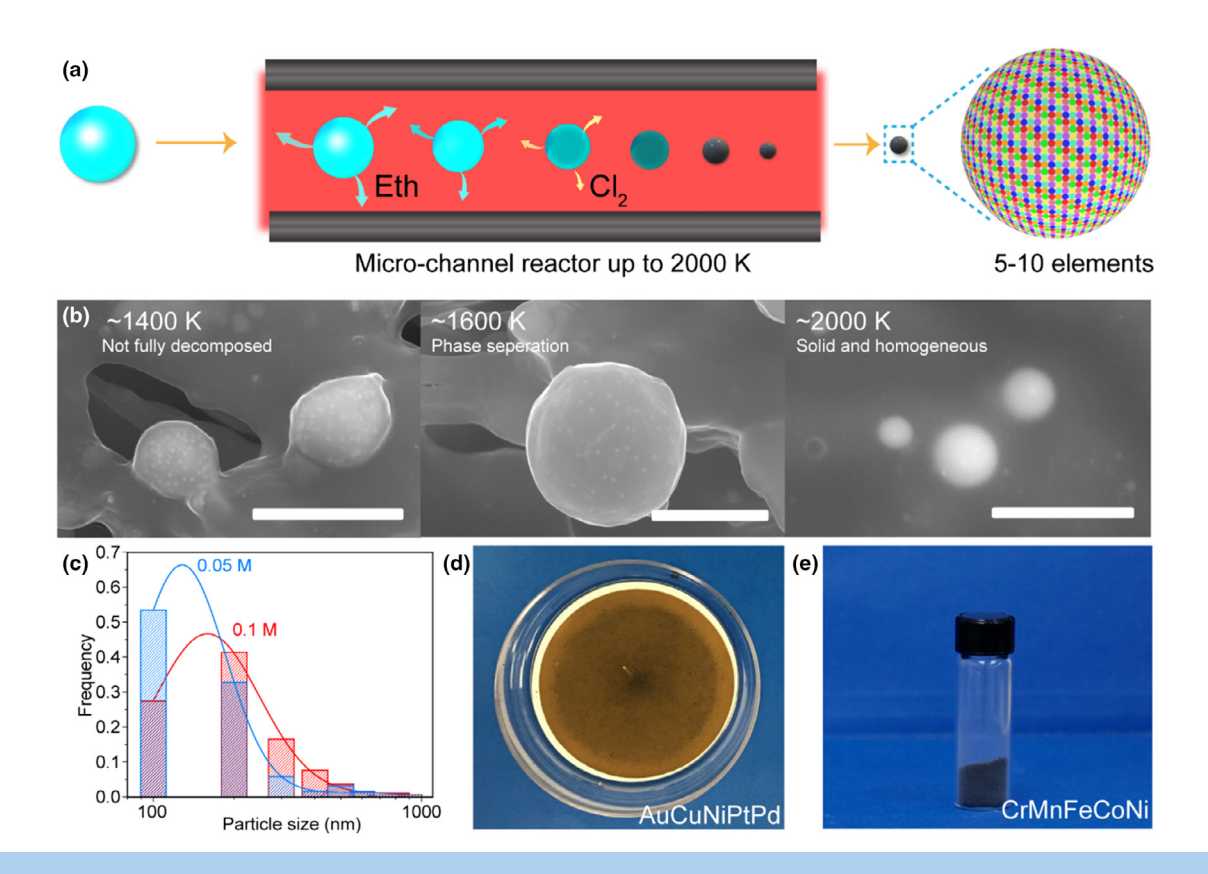


FIGURE 4

(a) Proposed mechanism of HEA formation inside the carbonized wood micro-channel reactor. (b) SEM of CoNiPdRuIr HEA particles synthesized at different temperatures. Scale bar: 1 µm. (c) Size distributions and log-normal fittings of the CoNiPdRuIr HEA nanoparticles synthesized at different precursor concentrations (0.05 M and 0.1 M). The fit parameters are listed in Tables S2 and S3. (d) AuCuNiPtPd HEA nanoparticles collected on a PVDF membrane after 5 min continuous synthesis. (e) CrMnFeCoNi HEA powder collected in a vial after 6 h continuous synthesis.

are thermally decomposed to form particles. As in regular aerosol synthesis [37], while the droplets flow in the micro-channels, the leftover solvent in the droplets rapidly evaporates upon heating so that each droplet evolves into a uniform and dense metal salt particle. Upon further heating, our hypothesis is that the metal salts decompose into metals and chlorine gas since the temperature exceeds their decomposition temperature. Additionally, because ~2000 K is above the melting point but below the boiling point of most metals, it is reasonable to assume that within each droplet the metallic elements tend to mix in the liquid phase to form a liquid metal alloy. Considering the residence time in the carbonized wood micro-channels is only ~16 ms. the liquid metal alloy particles are rapidly quenched down to room temperature after exiting the reactor, which enables the homogeneous elements mixing alloy state to be maintained, allowing us to collect HEA particles at room temperature.

We also conducted control experiments to understand the kinetic control of this droplet-to-particle process. Fig. 4b demonstrates how the temperature affects the nucleation of CoNiPdRuIr HEA nanoparticles. When the temperature of the carbonized wood micro-channel reactor is $\sim 1400 \, \text{K}$, it is too low to fully pyrolyze the droplets, resulting in particles that are in irregular shape. In addition, we clearly observed phase segregation in the nonuniform surfaces of these materials due to the low temperature, likely because only some noble metal salts with low decomposition temperatures (Pd, Ru, Ir) could be fully decom-

posed and nucleated, forming the bright dots shown on the surface of these materials in Fig. 4b. When we increased the temperature to $\sim\!1600\,\rm K$, regular round particles are produced, however, phase segregation can still be seen on the surface. In contrast, when the temperature is high enough (i.e., $\sim\!2000\,\rm K$), the decomposition rate is significantly enhanced and the decomposition of the metal salts can be completed (Fig. 4b). In addition, only at sufficiently high temperatures ($\sim\!2000\,\rm K$) can a homogeneous liquid alloy be formed. After rapid quenching, homogeneous high entropy mixing is obtained.

We further explored how the size distribution of the HEA nanoparticles (CoNiPdRuIr) could be tailored by tuning the concentration of the precursors. Fig. S12 shows HEA nanoparticles synthesized using precursors of different concentrations (0.1 M and 0.05 M) and their size distributions are shown in Fig. 4c. The results indicate that the particle size increases with the concentration of precursors, in which those made using a higher concentration (0.1 M) had a larger mean diameter of $\sim\!\!194\,\mathrm{nm}$ compared to those made with lower concentration (0.05 M), which were only 147 nm on average. These findings show that the particle size can be tuned kinetically.

The 2000 K droplet-to-particle synthesis demonstrates two obvious advantages: (1) it is substrate-free and (2) it is continuous and therefore amenable to large-scale fabrication. All of the particles can be collected in-line using a polyvinylidene fluoride (PVDF) membrane which is installed inside of a stainless-steel fil-

ter holder. Fig. 4d illustrates AuCuNiPtPd HEA nanoparticles collected on PVDF membrane for 5 min. Free powders of the HEA nanoparticles can then be obtained by carefully scratching the PVDF membrane with a spatula in the glovebox as we demonstrated by collecting CrMnFeCoNi HEA nanoparticles in a vial during their continuous synthesis over 6 hours at lab scale (5 L/min flow rate of Ar; Fig. 4e). At this flow rate, the production rate is on the order of ~ 100 mg/h.

Combining the advantages of low cost, simplicity, and low waste emission, the aerosol spray pyrolysis method is highly suitable for continuous large-scale manufacturing of high-quality HEA nanoparticles. For large-scale HEA production, a more powerful aerosol nebulizer, often used in the aerosol industry due to the higher aerosol generation rates, can be employed. Larger carbon materials with aligned micro-channels are expected as heating elements for potential large-scale manufacturing. Highly crystalline 3D printed rGO has such potential due to its long lifetime [38].

Conclusion

In this work, we demonstrate a droplet-to-particle synthesis technique by coupling an aerosol spray with a high-temperature (~2000 K) reactor made using carbonized balsa wood featuring numerous aligned micron-sized channels. The carbonized wood micro-channel reactor is driven by electrical Joule heating that can easily achieve a temperature greater than 2000 K with a high energy conversion efficiency. In addition, the 100-times reduction in the reactor geometry (micro-channel vs. tube furnace) ensures uniform heating for nanomaterial manufacturing. As a proof-of-concept demonstration, we synthesized uniform elemental mixed HEA and HEO nanoparticles in a substrate-free manner for the first time. The high temperature critically enables homogeneous elements mixing in the resultant nanoparticles and the short residence time suppresses particle growth and agglomeration. Compared with conventional pyrolysis, the 2000 K carbonized wood micro-channels provide several key features: (1) ≥2000 K heating for high-temperature chemistry; (2) more uniform and efficient heating with smaller channel dimensions; and (3) a shorter residence time on the scale of tens of milliseconds to enable transient nanomaterial structural stabilization and prevent particle agglomeration. In addition, this technique also offers good tunability in terms of flow rate, carrier gas, temperature, and precursor concentration. As a result, particles with a diverse array of compositions and sizes can be synthesized. Additionally, this droplet-to-particle method via a carbonized wood micro-channel reactor allows products to be collected continuously, which demonstrates the potential for large-scale high-temperature nanomaterial manufacturing.

Materials and methods

Material synthesis

All the precursors were purchased from Sigma Aldrich: palladium (II) chloride (\geq 99.9%), ruthenium(III) chloride hydrate (99.98%), iron(III) chloride hexahydrate (\geq 98%), nickel(II) chloride hexahydrate (\geq 98%), copper(II) chloride dihydrate (99.0%), iridium(III) chloride hydrate (99.9%), cobalt(II) chloride hexahydrate (98%), molybdenum(V) chloride (95%), tin(II) chloride

ride (98%), chloroplatinic acid hydrate (≥99.9%), manganese(II) chloride monohydrate (≥97%), gold(III) chloride trihydrate (≥99.9%) and zinc(II) nitrate hexahydrate (98%), manganese (II) nitrate hydrate (98%), cobalt(II) nitrate hexahydrate (≥98%), copper(II) nitrate hemi(pentahydrate) (98%), nickel(II) nitrate hexahydrate (>98.5%). Balsa wood was purchased from Specialized Balsa Wood, LLC and cut to a length of 100 mm, width of 40 mm, and thickness of \sim 6 mm (Fig. S1a and b). The balsa wood was first stabilized at 533 K for 2 h in air and then carbonized at 1273 K for 2 h in argon (Fig. S1c and d), after which its thickness shrank to \sim 4 mm. To make the carbonized wood into the heating element used in the aerosol spray high-temperature experiments, the carbonized wood first needs to be polished on each side using silicon carbon paper-600 with water in order to expose the channels by hand for \sim 1 min. The polished carbonized wood was then sonicated in ethanol several times to remove the polishing debris, followed by drying in an oven at 333 K for 20 min. For the aerosol spray pyrolysis in the carbonized wood micro-channel reactor, all HEA and HEO particles were synthesized based on the precursors of MCl_xH_v or M_x(NO₃)v, respectively, in equivalent ratios dissolved in ethanol. The precursor solutions were atomized into small droplets by a collision nebulizer from CH Technologies (USA), Inc. at a tunable flow rate with argon as the carrier gas. Nominally 1 µm droplets were generated, which were then flowed through a diffusion dryer, where most of the solvent was absorbed, leaving solid precursor particles which were then passed through the \sim 2000 K wood heating zone to produce the HEA/HEO particles. The final product was collected on a Millipore PVDF membrane with a pore size of $0.65\,\mu m$ installed inside of a 47 mm in-line stainless steel filter holder (PALL Corporation). Powders were obtained by scratching carefully from the PVDF membrane with a spatula in the glovebox. The carbonized wood was electrically heated to 2000 K by connecting two copper electrodes with silver paste. A Volteq HY 6020EX power supply acted as the external power source. The applied voltage ranged from 0 to 60 V and the current ranged from 0 to 20 A.

Material characterization

The microstructure and morphology of the prepared samples were measured by a Hitachi SU-70 FEG-SEM at 10 kV and a JEOL TEM/STEM ARM 200CF equipped with HAADF and annular bright field (ABF) detectors. A 22 mrad probe convergence angle was used to perform STEM imaging. HAADF images were acquired using the JEOL ARM 200CF with a 90 mrad inner-detector angle. An Oxford Xmax 100TLE windowless X-ray detector was used to collect the EDS results. XRD was performed using a D8 Advanced (Bruker AXS, WI, USA) with a scan rate of 3°/min.

Temperature measurement of the carbonized wood microchannel reactor

The temperature of the carbonized wood micro-channel reactor during heating was measured based on color ratio pyrometry using a Vision Research Phantom Miro M110 high-speed camera with video recorded at 4000 frames per second. Calibration was achieved by a Newport Oriel 67,000 Series Blackbody Infrared Light Source. By taking ratios of the raw channel intensities,

most dependent variables associated with the intensity can be eliminated except for those regarding the channel gain (ψ_i) , emissivity (ε) , and spectral response (χ_i) of the camera at individual wavelengths and channels [39]. Ratios for theoretical pixel intensity were calculated for the calibration temperature with Eq. (1).

$$\frac{I_{i}}{I_{j}} = \frac{\psi_{i} \int L(\varepsilon, \lambda, T) \chi_{i}(\lambda) d\lambda}{\psi_{j} \int L(\varepsilon, \lambda, T) \chi_{j}(\lambda) d\lambda} \tag{1}$$

in which I_i is the intensity of a channel. Calibration factors C_{gr} (green/red), C_{bg} (blue/green), and C_{br} (blue/red) can be obtained by comparing the measured values to the theoretical ones as shown in Eq. (2) [32].

$$\left(\frac{I_i}{I_j}\right) = C_{ij} \left(\frac{I_i}{I_j}\right)_{\phi}
\tag{2}$$

At each pixel, to recover values for the red, green, and blue channels, the demosaicing routine in MATLAB was used with the camera's Bayer color filter array. To estimate the temperature, three color ratios were used simultaneously by minimizing their summed error with a further thresholding used to eliminate summed errors corresponding to a temperature error of $>\sim 110~\rm K$. For the temperature profile, only unsaturated pixels above the black level and within the error threshold were used to report the mean and median temperatures of the frame for a contiguous area of at least 10 acceptable pixels. The temperature of the micro-channel reactor was calculated by fitting the emitted light spectra according to the gray body radiation and the following equation:

$$B_{\lambda}(\lambda, T) = \gamma \varepsilon_{gray} \frac{2hc^2}{\lambda^5} \frac{1}{e^{hc/\lambda k_B T} - 1}$$
 (3)

in which $k_{\rm B}$ is the Boltzmann constant, λ is the wavelength, h is Planck's constant, c is the speed of light, $\epsilon_{\rm gray}$ is the gray body emissivity and scaling constant γ and temperature T are fitting parameters for this equation.

Temperature mapping simulation methods

The numerical studies of the heat transfer from the heating sources (conventional furnace and carbonized wood) to the argon carrier gas were carried out in a commercial CFD package ANSYS-Fluent 18.1 (Double precision, 2D axisymmetric model). The *Re* number was calculated to be <2300 for both cases. Therefore, the laminar model was used for the simulations. The diameter of the conventional tube furnace was set to 2 cm, while the diameter of the wood micro-channel was set to an effective diameter of 192.8 μ m, which was calculated using $D = \frac{4A_C}{P}$, where A_C and P are the flow cross-sectional area and the wetted perimeter, respectively [40]. The length-to-diameter ratio of both the furnace tube and the carbonized wood micro-channel reactor was set to 20:1, and the inlet velocity was set to 0.265 m/s for both cases. The wall temperatures were set to 1300 K and 2000 K for the tube furnace and wood micro-channel, respectively.

The temperature change of the aerosol particle was simulated using the transient thermal model in ANSYS 18.1. The relative velocity between the aerosol particle and argon was assumed to be 0. The heat transfer between argon and the aerosol particles

was not considered. The diameter of the aerosol particle was set to $1\,\mu\text{m}.$

Acknowledgements

This work has no direct funding support. The authors acknowledge the use and support of the Maryland NanoCenter and its AIMLab. This work made use of the JEOL JEM-ARM200CF in the Electron Microscopy Service (Research Resources Center, UIC). The acquisition of the UIC JEOL JEM-ARM200CF was supported by an MRI-R2 grant from the National Science Foundation (NSF) (DMR-0959470). R.S.Y. acknowledges financial support from NSF DMR-1620901. Z.H.'s microscopy characterization efforts were supported by NSF-DMR-1809439.

Author contributions

L.H. and X.W. conceived the idea and designed the present work. X.W., H.Q., G.Z., and Q.X. carried out the experiments. Z.H., Y. Y., and R.S.Y. performed detailed microscopic characterization. Y.P., C.Z., and B.Y. performed the numerical studies of the heat transfer performances. X.W., D.K. and M.Z. conducted high-temperature characterization. All authors discussed the results and contributed to the final manuscript.

Competing interests

The authors declare no competing interests.

Data and materials availability

All data are available in the manuscript and the supporting materials.

Appendix A. Supplementary data

Supplementary data to this article can be found online at https://doi.org/10.1016/j.mattod.2019.11.004.

References

- [1] J. Lu et al., Nat. Nanotechnol. 11 (12) (2016) 1031.
- [2] A.I. Kuznetsov et al., Science 354 (2016) 6314.
- [3] M. Auffan et al., Nat. Nanotechnol. 4 (10) (2009) 634.
- [4] W. Jiang et al., Nat. Nanotechnol. 3 (3) (2008) 145.
- [5] R.C. Jin et al., Chem. Rev. 116 (18) (2016) 10346.
- [6] M.B. Cortie, A.M. McDonagh, Chem. Rev. 111 (6) (2011) 3713.
- [7] K.L. Ding et al., Science 362 (6414) (2018) 560.
- [8] Y.J. Zhu et al., Adv. Energy Mater. 7 (2017) 7.
- [9] S.E. Skrabalak, K.S. Suslick, J. Am. Chem. Soc. 128 (39) (2006) 12642.
- [10] H.X. Xu et al., Adv. Mater. 24 (45) (2012) 6028.
- [11] Y.H. Xu et al., Nano Lett. 13 (2) (2013) 470.
- [12] J. Leng et al., Chem. Soc. Rev. 48 (11) (2019) 3015.
- [13] Z. Jin et al., Angew. Chem. Int. Ed. 51 (26) (2012) 6406.
- [14] L. Kuai et al., Angew. Chem. Int. Ed. 53 (29) (2014) 7547.
- [15] Y.J. Hong et al., Adv. Mater. 25 (16) (2013) 2279.
- [16] J. Liu et al., Energy Environ. Sci. 4 (3) (2011) 885.
- [17] J.C. Guo et al., Adv. Funct. Mater. 22 (4) (2012) 803.
- [18] B. Xia et al., Adv. Mater. 13 (23) (2001) 1744.
- [19] N.E. Motl et al., J. Mater. Chem. A 1 (17) (2013) 5193.
- [20] S.M. Oh et al., Adv. Funct. Mater. 20 (19) (2010) 3260.
- [21] S.H. Choi et al., Nanoscale 5 (17) (2013) 7867.
- [22] D.S. Jung et al., Nano Lett. 13 (5) (2013) 2092.
- [23] G.Q. Jian et al., Angew. Chem. Int. Ed. 52 (37) (2013) 9743.
- [24] G.Q. Jian et al., Adv. Funct. Mater. 23 (10) (2013) 1341.
- [25] J. Gild et al., J. Eur. Ceram. Soc. 38 (10) (2018) 3578.
- [26] J. Gild et al., Sci. Rep.-UK 6 (2016).
- [27] Y.G. Yao et al., Science 359 (6383) (2018) 1489.
- [28] S.C. Jiang et al., Scripta Mater. 142 (2018) 116.

- [29] Y.F. Ye et al., Mater. Today 19 (6) (2016) 349.
- [30] T. Loffler et al., Adv. Energy Mater. 8 (2018) 34.
- [31] S.E. Johnson, F.A. Kamke, J. Adhes. 40 (1) (1992) 47.
- [32] R.J. Jacob et al., J. Appl. Phys. 123 (2018) 11.
- [33] Q.F. Wu et al., Metall. Mater. Trans. A 49A (10) (2018) 4986.
- [34] L. Lu et al., Science 304 (5669) (2004) 422.
- [35] H. Van Swygenhoven, J.R. Weertman, Mater. Today 9 (5) (2006) 24.
- [36] A. Sarkar et al., J. Eur. Ceram. Soc. 37 (2) (2017) 747.
- [37] K. Okuyama, I.W. Lenggoro, Chem. Eng. Sci. 58 (3–6) (2003) 537.
- [38] W.Z. Bao et al., Adv. Mater. 28 (23) (2016) 4684.
- [39] T.R. Fu et al., J. Heat Transfer Trans. ASME 132 (2010) 5.
- [40] F.P.I.T.L. Bergman, D.P. Dewitt, A.S. Lavine, Fundermentals of Heat and Mass Transfer, John Wiley & Son, 2011.